

Electronic Supporting Information

Cooperativity in spin crossover materials as ligand's responsibility – Investigations on the Fe(II) - 1,3-bis((1*H*-tetrazol-1-yl)methyl)bicyclo[1.1.1]pentane system

Christian Knoll,^a Marco Seifried,^a Gerald Giester,^b Jan M. Welch,^c Werner Artner,^d Klaudia Hradil,^d Michael Reissner,^e Danny Müller,^{a*} and Peter Weinberger^a

^a Institute of Applied Synthetic Chemistry, TU Wien, Getreidemarkt 9/163-AC, 1060 Vienna, Austria

^b Department of Mineralogy and Crystallography, University of Vienna, Althanstraße 14 (UZA 2), 1090 Vienna, Austria

^c Atominstytut, TU Wien, Stadionallee 2, 1020 Vienna, Austria

^d X-Ray Center, TU Wien, Getreidemarkt 9, 1060 Vienna, Austria

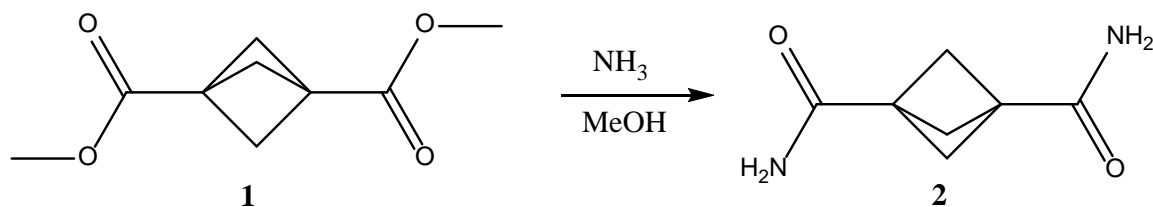
^e Institute of Solid State Physics, TU Wien, Wiedner Hauptstraße 8-10/138, 1040 Vienna, Austria

Content

Experimental section.....	2
Methods	4
Experimental	4
Nuclear magnetic resonance spectroscopy (NMR).....	4
Magnetic moment (VSM).....	4
UV-Vis-NIR spectroscopy.....	5
Infrared Spectroscopy	7
<i>Mid-range infrared spectroscopy (MIR)</i>	7
<i>Far-range infrared spectroscopy (FIR)</i>	7
Single crystal X-ray diffraction (sc-XRD)	11
Solvate determination by ¹ H-NMR.....	13
Thermogravimetry.....	14
Powder X-ray diffraction (XRD)	15
Computational details	16
References.....	18

Experimental section

Bicyclo[1.1.1]pentane-1,3-dicarboxamide (2)



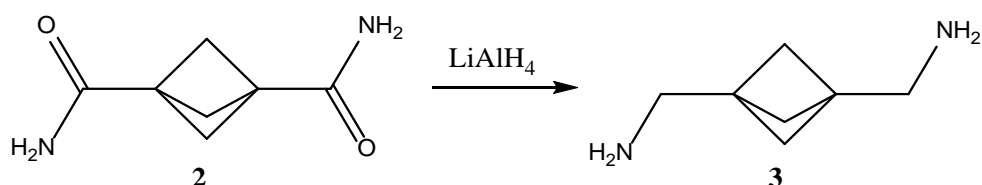
Dimethyl bicyclo[1.1.1]pentane-1,3-dicarboxylate was prepared according to literature.¹

5.1 g (27.4 mmol, 1 eq.) dimethyl bicyclo[1.1.1]pentane-1,3-dicarboxylate were suspended at room temperature in 200 mL of cold-saturated ammonia solution in methanol and stirred overnight. The white precipitate was separated, washed with methanol and dried in vacuum, yielding the product as a white solid.

Yield: 3.8 g 88.7 %

^1H NMR (400 MHz, DMSO-d_6 , δ): 3.60 (s, 1H), 2.12 (s, 2H), 2.01 (s, 2H); $^{13}\text{C}\{^1\text{H}\}$ NMR (101 MHz, DMSO-d_6 , δ): 171.21, 51.68, 51.19; MIR (ν , cm^{-1}): 3319 (m), 3148 (m), 2996 (w), 1628 (s), 1429 (s), 1228 (m), 1156 (m), 1123(m), 832 (w), 699 (s), 583 (w), 459 (s); EA: Calc. for $\text{C}_7\text{H}_{10}\text{N}_2\text{O}_2$: C 54.54, H 6.54, N 18.17, O 20.76; found C 53.93, H 6.51, N 17.13, O 20.70

Bicyclo[1.1.1]pentane-1,3-diylidimethanamine (3)

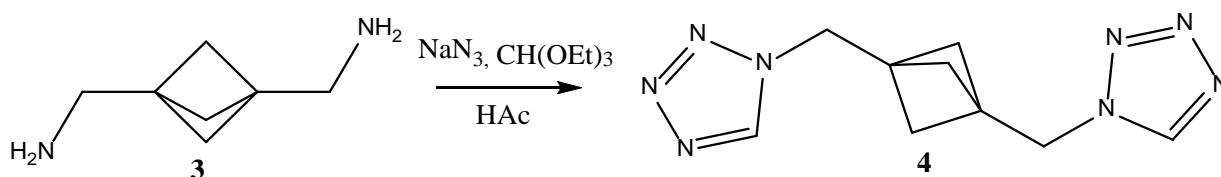


3.73 g (24.2 mmol, 1 eq.) bicyclo[1.1.1]pentane-1,3-dicarboxamide were suspended in dry THF and 30 mL (2.75 g, 72.6 mmol, 3 eq.) lithium aluminum hydride as 2.4 M solution in THF were added via a syringe. After complete addition the white suspension was stirred at room temperature for 10 minutes and heated to reflux for 24 hours. After cooling to room temperature, the excess of lithium aluminum hydride was quenched with 12 mL saturated sodium chloride solution. The suspension was filtered over a pad of Celite, washed twice with THF, evaporated under reduced pressure, suspended in methylene chloride, dried over magnesium sulfate and evaporated again, yielding a slightly yellow oil. The product was used without further purification.

Yield: 2.5 g 80.6 %

^1H NMR (400 MHz, CD_2Cl_2 , δ): 2.64 (s, 4H), 1.45 (s, 6H); $^{13}\text{C}\{^1\text{H}\}$ NMR (101 MHz, CD_2Cl_2 , δ): 47.16, 44.41, 41.40; MIR (ν , cm^{-1}): 3279 (w), 2956 (s), 2901 (s), 2862 (s), 1602 (m), 1445 (w), 1345 (w), 1263 (s), 1138 (m), 1100 (m), 849 (s), 642 (m),

1,3-bis((1H-tetrazol-1-yl)methyl)bicyclo[1.1.1]pentane (4)



2.5 g (19.5 mmol, 1 eq.) bicyclo[1.1.1]pentane-1,3-diyldimethanamine 3.8 g (58.5 mmol, 3 eq.) sodium azide and 10 mL (9 g, 60 mmol, 3.1 eq.) triethyl orthoformate were suspended in 70 mL acetic acid and stirred for 18 h at 95 °C. The solution was evaporated under reduced pressure at 65 °C, the residue was suspended in water, precipitating a white solid. The product was separated and dried. The aqueous filtrate was neutralized with sodium hydroxide and a second fraction of the product was isolated.

Yield: 1.6 g 34.9 %

¹H NMR (400 MHz, DMSO-d₆, δ): 9.35 (s, 2H), 4.61 (s, 4), 1.55 (s, 6H) ppm; ¹³C{¹H} NMR (101 MHz, DMSO-d₆, δ): 143.83, 48.89, 48.26, 37.91; MIR (ν, cm⁻¹): 3122 (w), 3103 (m), 2980 (m), 2912 (m), 2875 (w), 1477 (m), 1436 (m), 1424 (s), 1261 (s), 1167 (s), 1110 (s), 1099 (s), 1022 (w), 967 (s), 914 (m), 890 (s), 738 (m), 721 (m), 686 (s), 653 (m), 543 (w); EA: Calc. for C₉H₁₂N₈: C 46.54, H 5.21, N 48.25; found C 46.51, H 5.12, N 46.9

[Fe(ppditz)₃](BF₄)₂ (5)

49 mg (0.22 mmol, 1 eq.) iron(II) tetrafluoroborate and 150 mg (0.65 mmol, 3 eq.) tricyclo[1.1.1.0^{1,3}]pentane ditetrazole were suspended in 5 mL of dry, degassed acetonitrile. The reaction was kept at 55 °C for 18 h. The solid was separated using a stainless steel pressure filter, washed with 20 mL of acetonitrile and afterwards with 25 mL of diethyl ether. The product was dried in vacuum and obtained as white powder.

Yield: 96 mg 47.1 %

MIR (ν, cm⁻¹): 3139 (w), 1504 (w); EA: Calc. for C₂₇H₃₆B₂F₈FeN₂₄: C 35.01, H 3.92, N 36.30; found C 35.00, H 3.77, N 36.24

[Fe(ppditz)₃](ClO₄)₂ (6)

55 mg (0.22 mmol, 1 eq.) iron(II) perchlorate and 150 mg (0.65 mmol, 3 eq.) tricyclo[1.1.1.0^{1,3}]pentane ditetrazole were suspended in 5 mL of dry, degassed acetonitrile. The reaction was kept at 55 °C for 18 h. The solid was separated using a stainless steel pressure filter, washed with 20 mL of acetonitrile and afterwards with 25 mL of diethyl ether. The product was dried in vacuum and obtained as white powder.

Yield: 80 mg 38.2 %

MIR (ν, cm⁻¹): 3133 (w), 1503 (w); EA: Calc. for C₂₇H₃₆Cl₂FeN₂₄O₈: C 34.08, H 3.81, N 35.33, O 13.45; found C 33.12, H 3.72, N 34.16, O 14.69

[Fe(ppditz)₃](PF₆)₂ (7)

74 mg (0.22 mmol, 1 eq.) iron(II) hexafluorophosphate and 150 mg (0.65 mmol, 3 eq.) tricyclo[1.1.1.0^{1,3}]pentane ditetrazole were suspended in 5 mL of dry, degassed acetonitrile. The reaction was kept at 55 °C for 18 h. The solid was separated using a stainless steel pressure filter, washed with 20 mL of acetonitrile and afterwards with 25 mL of diethyl ether. The product was dried in vacuum and obtained as white powder.

Yield: 45 mg 19.6 %

MIR (ν, cm⁻¹): 3147 (w), 1504 (w); EA: Calc. for C₂₇H₃₆F₁₂FeN₂₄P₂: C 31.11, H 3.48, N 32.25; found C 30.35, H 3.43, N 31.13

Methods

Experimental

If not otherwise stated, all operations involving iron(II) were carried out under inert-gas atmosphere (argon 5.0). The used glassware was oven-dried at 120 °C before use for at least 2 hours. All solvents for the complexation reactions were dried before use and stored over molecular-sieve 3 Å under argon.²

Unless otherwise stated, all commercially available compounds were purchased from Sigma Aldrich.

Tetrazoles and their derivatives, especially in combination with perchlorates, are potentially shock-sensitive or explosive compounds and should therefore be handled with great care and under appropriate safety precautions!

Nuclear magnetic resonance spectroscopy (NMR)

All spectra were recorded in dry, deuterated solvents as indicated.

¹H and ¹³C NMR spectra were recorded on a Bruker Avance UltraShield 400 MHz. All NMR chemical shifts are reported in ppm; ¹H and ¹³C shifts are reported against the residual solvent resonance.

Magnetic moment (VSM)

The magnetic moment of the Fe(II)-complexes was measured using a Physical Property Measurement System (PPMS®) by *Quantum Design*. The experimental setup consisted of a vibrating sample magnetometer attachment (VSM), bearing a brass-sample holder with a quartz-glass powder container. The moment was determined in an external field of 1 T in the range of 10 K to 300 K.

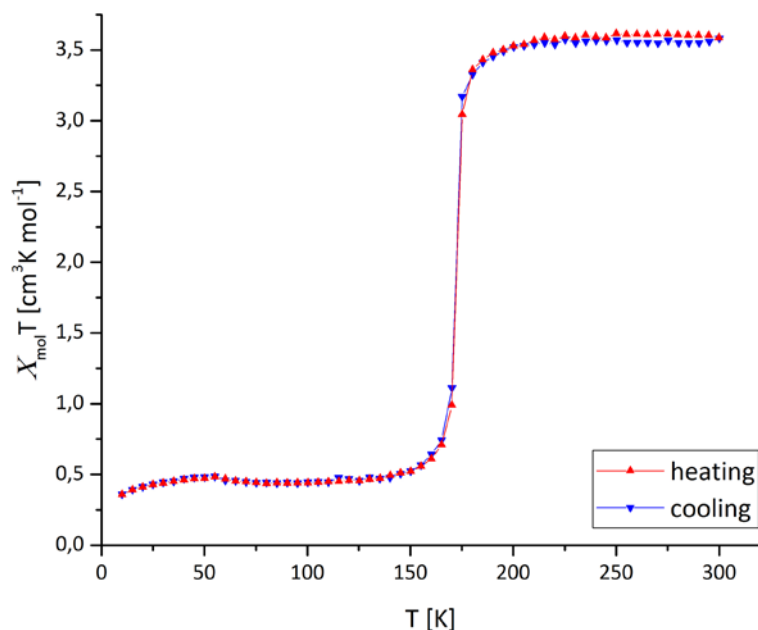


Fig. S1 Temperature dependent magnetic susceptibility of **5**, obtained in cooling-mode (blue) and heating mode (red)

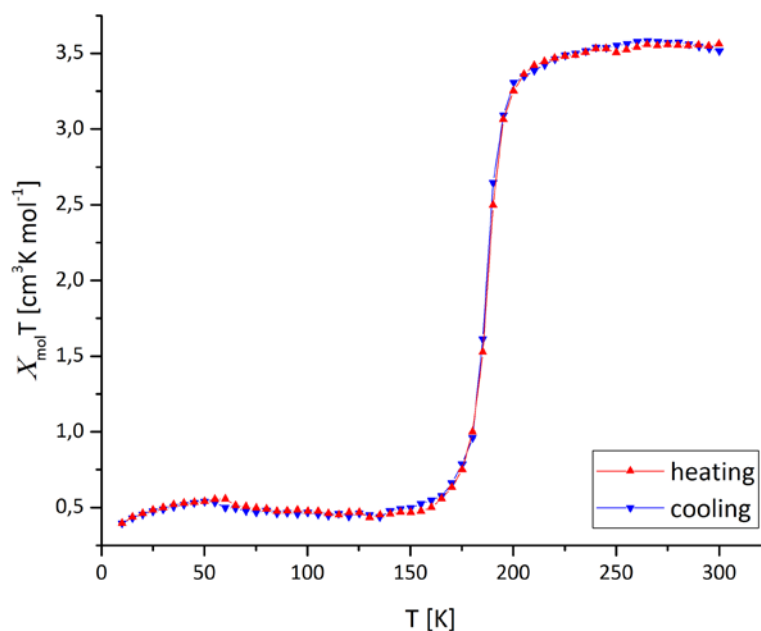


Fig. S2 Temperature dependent magnetic susceptibility of **6**, obtained in cooling-mode (blue) and heating mode (red)

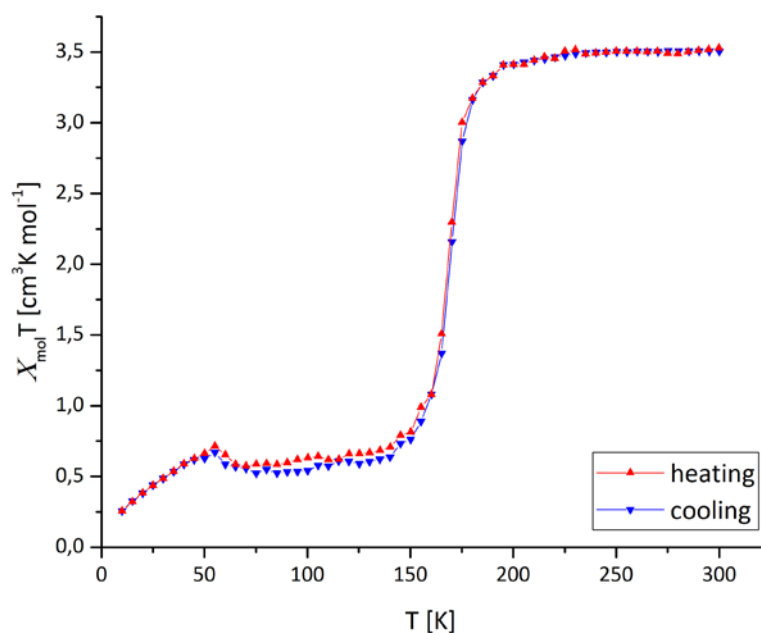


Fig. S3 Temperature dependent magnetic susceptibility of **7**, obtained in cooling-mode (blue) and heating mode (red)

UV-Vis-NIR spectroscopy

Variable temperature solid state UV-Vis-NIR spectra were recorded on a Perkin-Elmer Lambda 900 spectrophotometer between 300 and 1600 nm in diffuse reflectance against BaSO₄ as background. A Harrick coolable/heatable powder sample holder in "Praying Mantis" configuration was used.

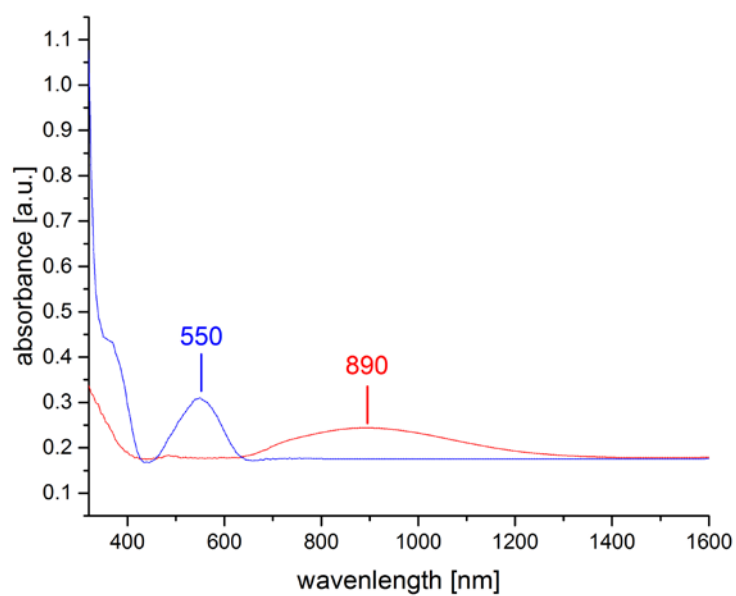


Fig. S4 UV-VIS-NIR spectra for **5** in the high-spin (red, 298 K) and low-spin state (blue, 100 K) with spin-state characteristic absorption maxima

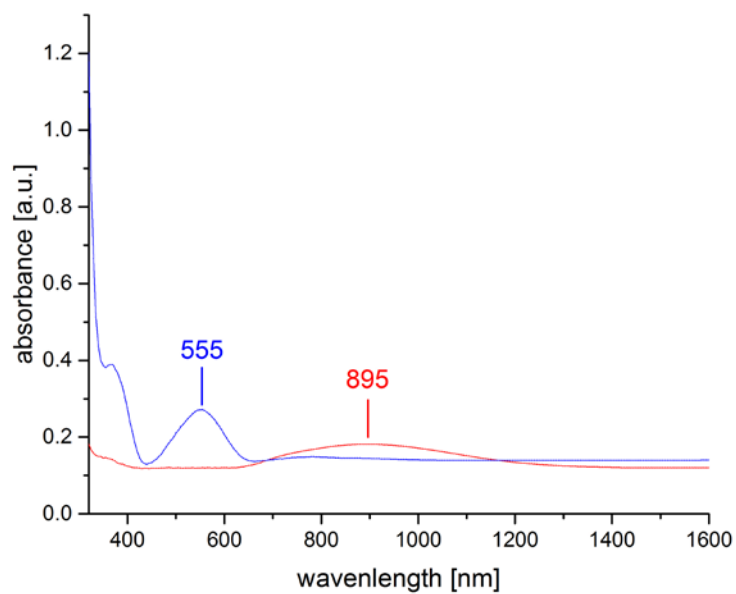


Fig. S5 UV-VIS-NIR spectra for **6** in the high-spin (red, 298 K) and low-spin state (blue, 100 K) with spin-state characteristic absorption maxima

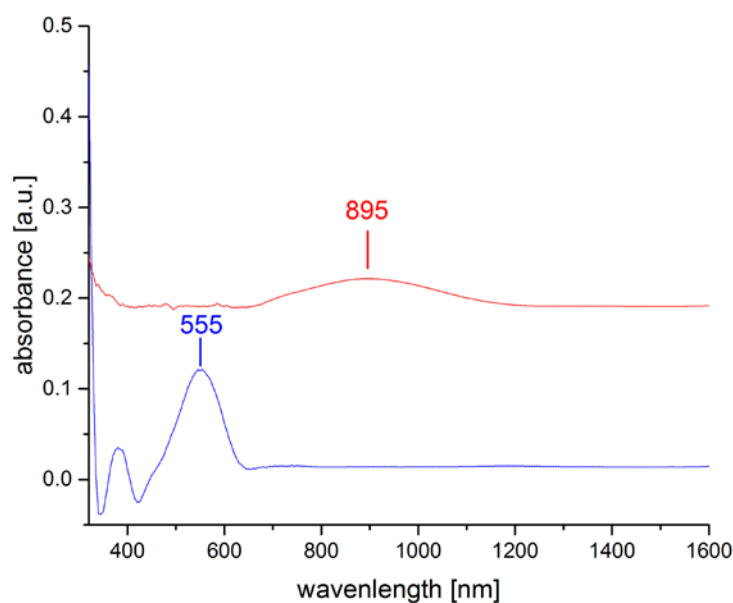


Fig. S6 UV-VIS-NIR spectra for **7** in the high-spin (red, 298 K) and low-spin state (blue, 100 K) with spin-state characteristic absorption maxima

Infrared Spectroscopy

Mid-range infrared spectroscopy (MIR)

Mid-range infrared spectra were recorded at ambient conditions in ATR technique within the range of 4000 - 450 cm^{-1} using a Perkin-Elmer Spectrum Two FTIR spectrometer with an UATR accessory attached. If not otherwise stated, the background was measured with opened anvil versus ambient air.

For the measurement of mid-range infrared spectra at different temperatures a Perkin-Elmer spectrum 400 fitted with a coolable/heatable Specac transmission unit was used.

As only quantitative information about the wavenumbers of certain bands is of interest, but not the information about the absolute intensities of the bands, an automatic baseline correction and normalization procedure implemented in the software Spectrum vers. 10.4.1.262 PerkinElmer® was applied on the spectra.

Far-range infrared spectroscopy (FIR)

For the measurement of far-range infrared spectra at different temperatures a Perkin-Elmer spectrum 400 fitted with a coolable/heatable PIKE Gladi ATR-Unit was used within the range of 700 - 180 cm^{-1} .

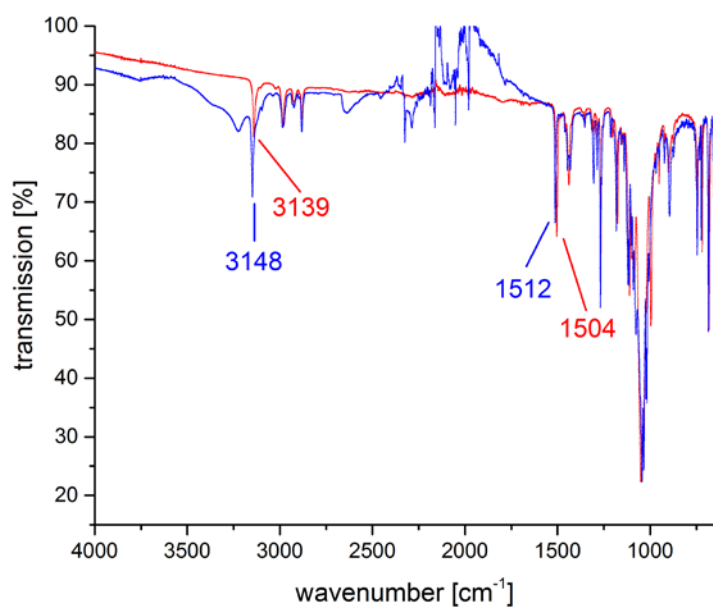


Fig. S7 MIR spectra for **5** in the high-spin (red, 298 K) and low-spin state (blue, 100 K) with labelled shifts of the tetrazolic ν_{CH} and ν_{NN} vibrational modes

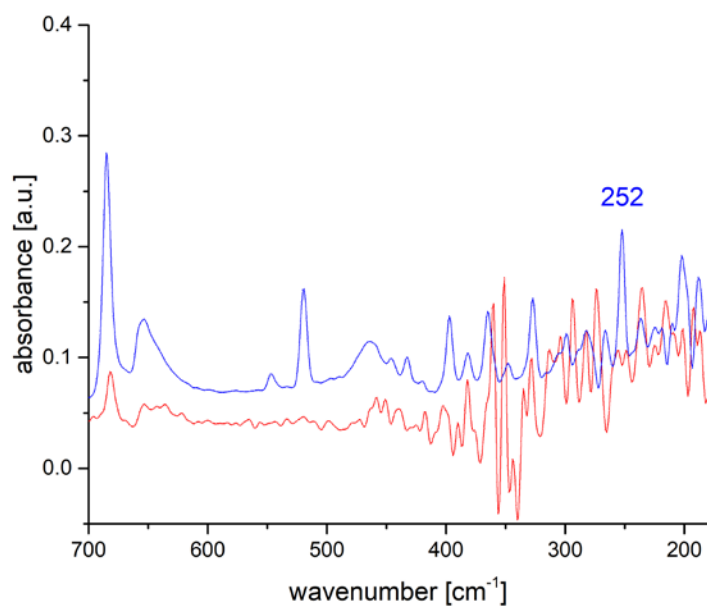


Fig. S8 FIR spectra for **5** in the high-spin (red, 298 K) and low-spin state (blue, 100 K) with labelled spin-state characteristic vibrational modes

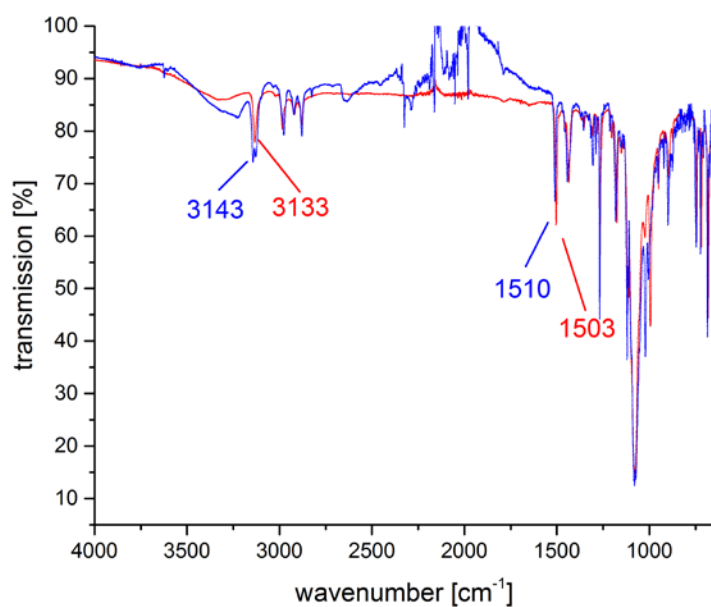


Fig. S9 MIR spectra for **6** in the high-spin (red, 298 K) and low-spin state (blue, 100 K) with labelled shifts of the tetrazolic ν_{CH} and ν_{NN} vibrational modes

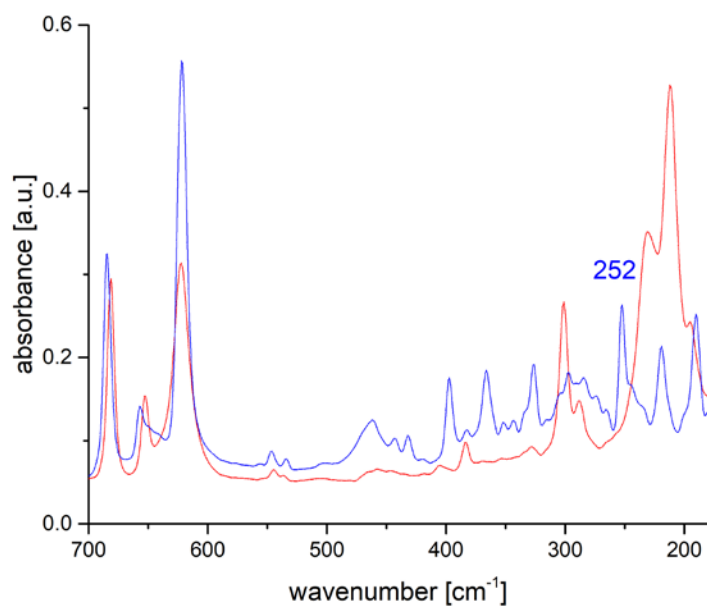


Fig. S10 FIR spectra for **6** in the high-spin (red, 298 K) and low-spin state (blue, 100 K) with labelled spin-state characteristic vibrational modes

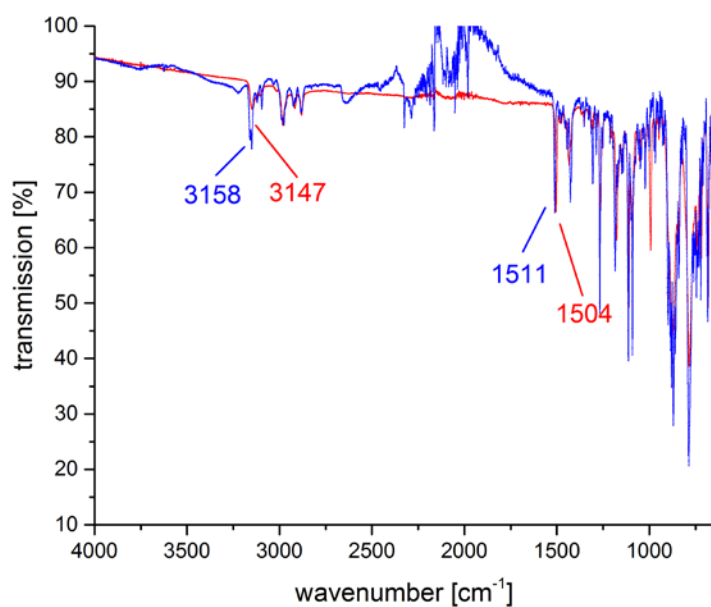


Fig. S11 MIR spectra for **7** in the high-spin (red, 298 K) and low-spin state (blue, 100 K) with labelled shifts of the tetrazolic ν_{CH} and ν_{NN} vibrational modes

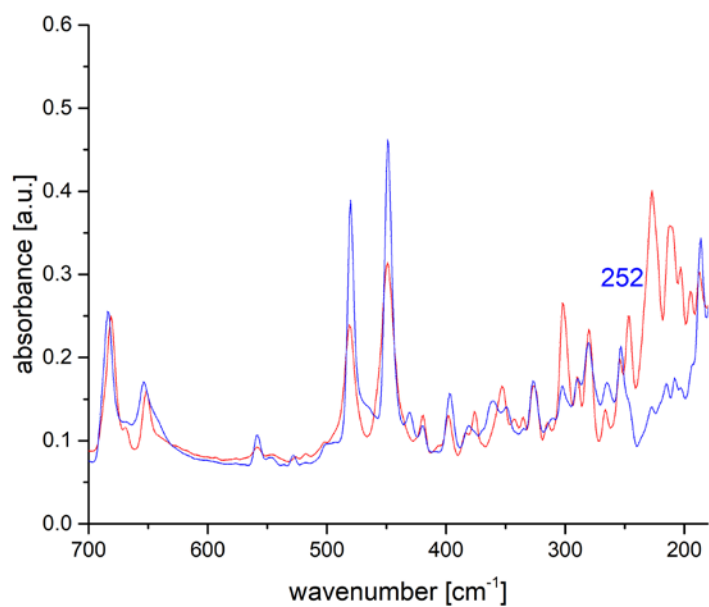


Fig. S12 FIR spectra for **7** in the high-spin (red, 298 K) and low-spin state (blue, 100 K) with labelled spin-state characteristic vibrational modes

Single crystal X-ray diffraction (sc-XRD)

Single crystals were attached to a glass fiber by using perfluorinated oil and were mounted on a Bruker KAPPA APEX II diffractometer equipped with a CCD detector with Mo K α radiation (Incoatec Microfocus Source $I_{\mu S}$: 30 W, multilayer mirror, $\lambda=0.71073$ Å). Data were collected at 100 K and 200 K (Cryostream 800, Oxford Cryosystems) in a dry stream of nitrogen. Redundant data sets up to $2\theta = 55^\circ$ were collected. Data were reduced to intensity values by using SAINT-Plus³, and an absorption correction was applied by using the multi-scan method implemented by SADABS.³ Initial models of the complexes at 200 K were derived from models based on 100 K data. For the iron(II) complexes, protons were placed at calculated positions and refined as riding on the parent C atoms. All non-H atoms were refined with anisotropic displacement parameters.

Table S1 Crystallographic data for complexes **5** and **6**

	5, HS	5, LS	6, HS	6, LS
Formula	C ₂₇ H ₃₆ N ₂₄ B ₂ F ₈ Fe	C ₂₇ H ₃₆ N ₂₄ B ₂ F ₈ Fe	C ₂₇ H ₃₆ N ₂₄ Cl ₂ O ₈ Fe	C ₂₇ H ₃₆ N ₂₄ Cl ₂ O ₈ Fe
M _r	926.19	926.19	951.48	951.48
Habit, color	Platelet, colorless	Platelet, pink	Platelet, colorless	Platelet, pink
Crystal system	Trigonal	Trigonal	Trigonal	Trigonal
Space group	<i>P</i> $\bar{3}c1$	<i>P</i> $\bar{3}c1$	<i>P</i> $\bar{3}c1$	<i>P</i> $\bar{3}c1$
a [Å]	11.3101(16)	11.1171(16)	11.2861(3)	11.1004(7)
b [Å]	11.3101(16)	11.1171(16)	11.2861(3)	11.1004(7)
c [Å]	19.393(4)	19.268(4)	19.6585(6)	19.4074(15)
γ [°]	120	120	120	120
V [Å ³]	2148.37	2062.29	2168.55	2070.98
Z	2	2	2	2
T [K]	200	100	250	100
ρ_{calc} [g cm ⁻³]	1.432	1.492	1.457	1.526
μ [mm ⁻¹]	0.439	0.458	0.545	0.571
Meas. refl.	16410	21198	51862	48146
Unique refl.	1781	1722	2219	2123
R _{int}	0.0625	0.0889	0.0563	0.0988
F(000)	948	948	980	980
R ₁	0.0508	0.0582	0.0446	0.0953
wR ₂	0.1487	0.1287	0.1311	0.1876
Goodness-of-fit	1.156	1.107	1.057	1.264
No. of parameters	108	109	108	108
CCDC-number	1564873	1564874	1564875	1564876

Table S2 Selected bond-lengths for complexes **5** and **6** in the high-spin and low-spin state

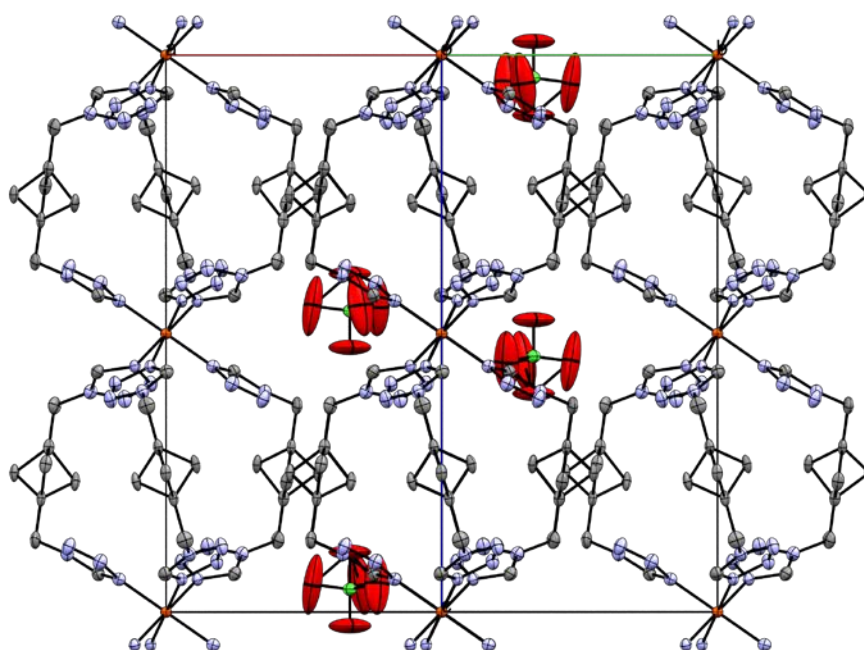
	Fe-Fe [Å]	Fe-N4 [Å]	N4-N3 [Å]	N3-N2 [Å]	N2-N1 [Å]	N4-C1 [Å]	C1-N1 [Å]	N1-C2 [Å]	C2-C3 [Å]	C3-C4 [Å]
5 , HS	9.634	2.1864	1.3563	1.2909	1.3475	1.3128	1.3219	1.4684	1.5038	1.5459
5 , LS	9.697	2.0207	1.3701	1.2831	1.3595	1.3230	1.3302	1.4665	1.5026	1.5494
6 , HS	9.829	2.1788	1.3547	1.2840	1.3417	1.3204	1.3187	1.4678	1.4981	1.5436
6 , LS	9.704	2.0255	1.3608	1.2897	1.3606	1.3191	1.3265	1.4561	1.5049	1.5494

Table S3 Selected bond-lengths and bond-angles for complexes **5** and **6** in the low-spin state

	N4-Fe-N4[°]	N4-C1-N1 [°]	N1-C2-C3 [°]	C3-C4-C3 [°]
5 , HS	92.16	108.67	109.67	73.95
5 , LS	91.58	108.03	109.41	74.11
6 , HS	91.59	108.50	110.19	73.86
6 , LS	91.28	108.28	110.61	73.50

Table S4 Calculated voids and electrons by SQUEEZE

	5 , HS	5 , LS	6 , HS	6 , LS
Void-volume [Å ³]	179.6	156.5	174.7	150.7
Electrons found	21.6	59.1	42.4	39.9

**Fig. S13** View of **6** along the crystallographic *a*-axis with the infinite *ppdtiz* chains

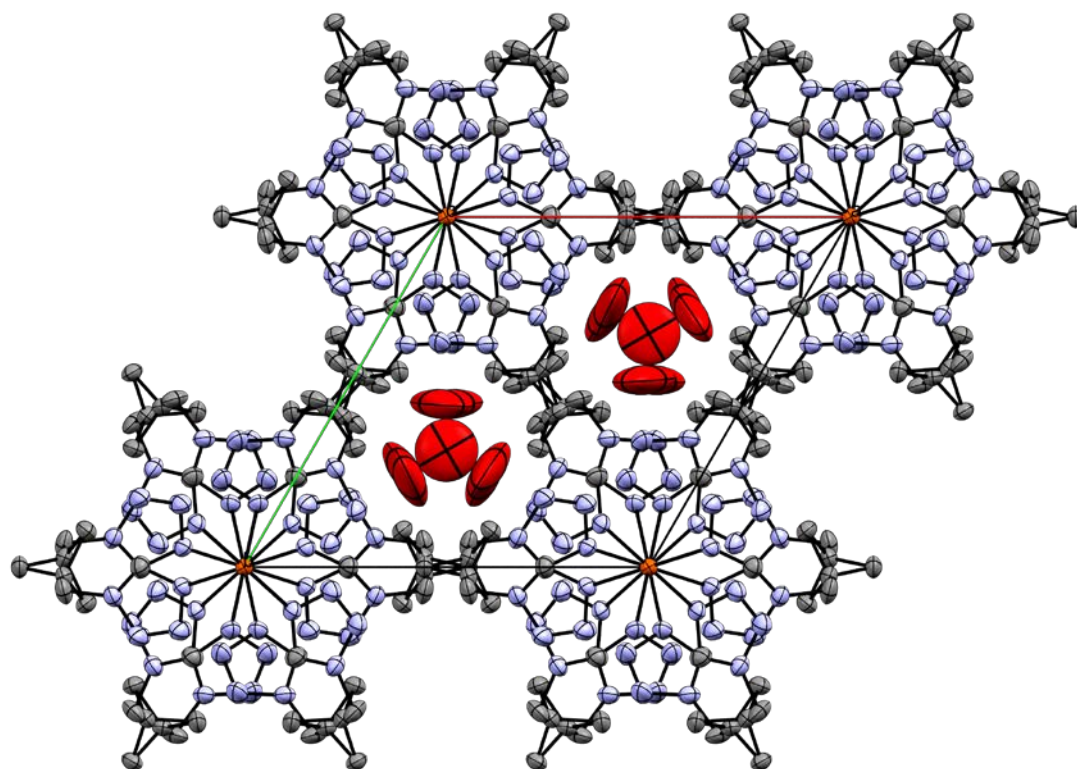


Fig. S14 View of **6** along the crystallographic *c*-axis with the Fe-atoms located at the corners of the elemental cell. The channels between the *ppdtitz* chains are occupied by the anions

Solvate determination by $^1\text{H-NMR}$

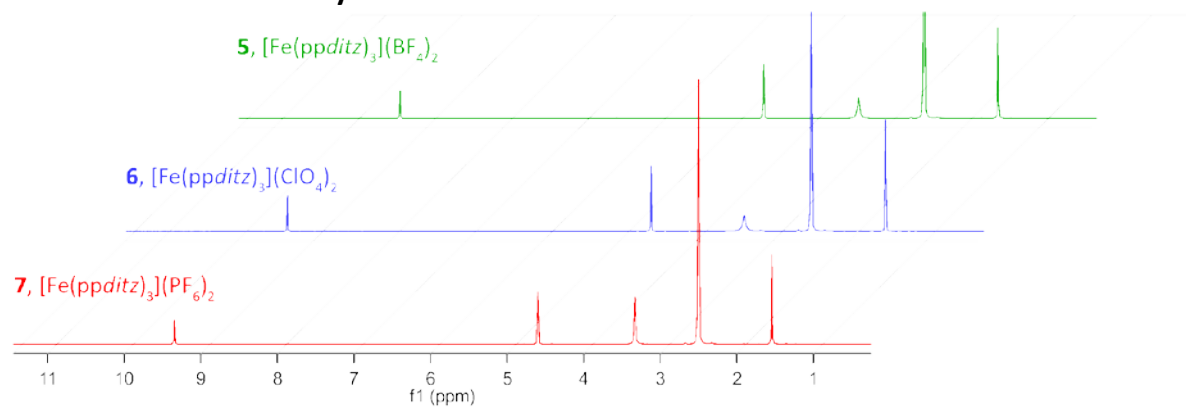


Fig. S15 $^1\text{H-NMR}$ spectra of compounds **5-7**, showing no solvate signals. (DMSO- d_6 at 2.50 ppm, H_2O from DMSO- d_6 at 3.3 ppm)

Thermogravimetry

For thermogravimetric analysis a Mettler Toledo TGA system with a heating rate of 10 K/min under N₂ atmosphere was used between 25 °C and 500°C.

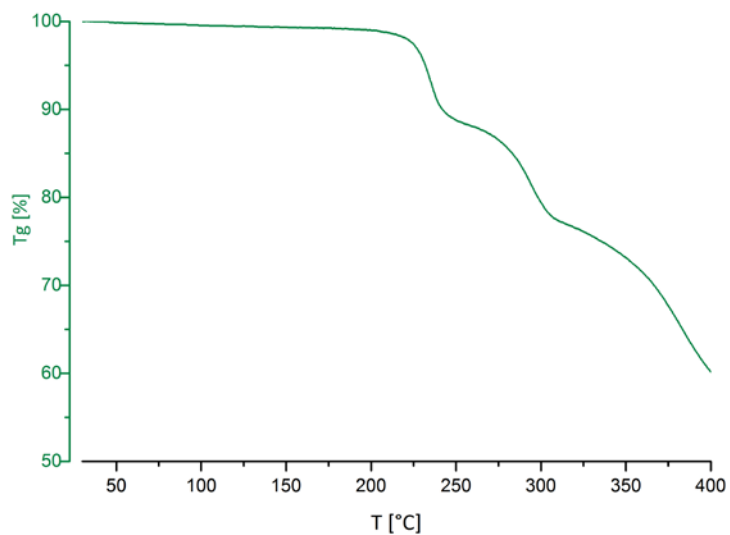


Fig. S16 Thermogravimetric decomposition of **5**

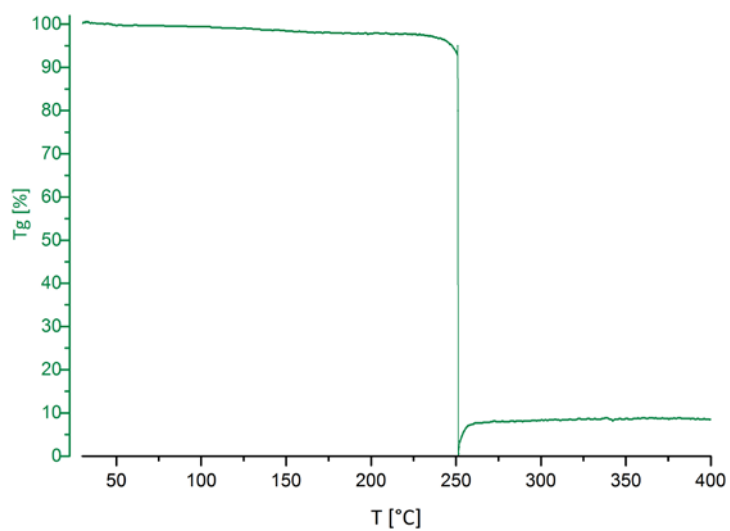


Fig. S17 Thermogravimetric decomposition of **6**

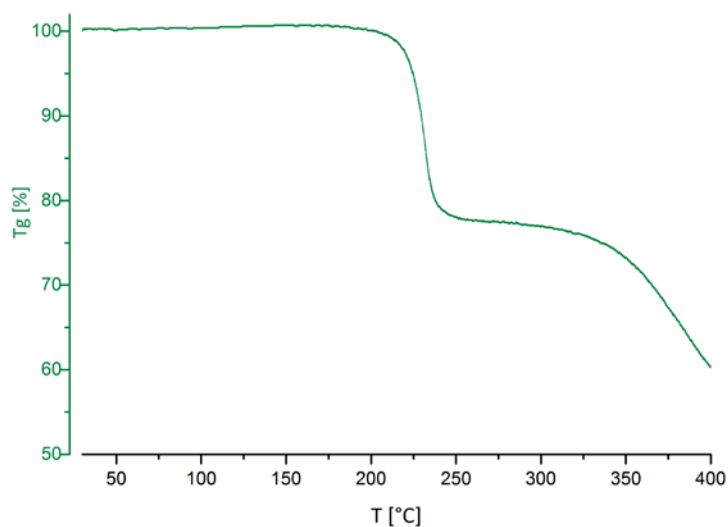


Fig. S18 Thermogravimetric decomposition of **7**

Powder X-ray diffraction (XRD)

The powder X-ray diffraction measurements were carried out on a PANalytical X'Pert diffractometer in Bragg-Brentano geometry using Cu $K_{\alpha 1,2}$ radiation, an X'Celerator linear detector with a Ni-filter, sample spinning with back loading zero background sample holders and $2\theta = 4-90^\circ$ $T = 297$ K at the X-ray Center at TU Wien. The diffractograms were evaluated using the PANalytical program suite HighScorePlus v3.0d. A background correction and a $K_{\alpha 2}$ strip were performed.

As all spectroscopic and magnetic investigations have been performed on powder samples, it was verified that the powder samples of the complex were identical to the single crystals, used for the structure determination. For this purpose powder X-ray diffraction revealed an excellent fit to an one-phase model, indicating the absence of any other detectable crystalline phases.

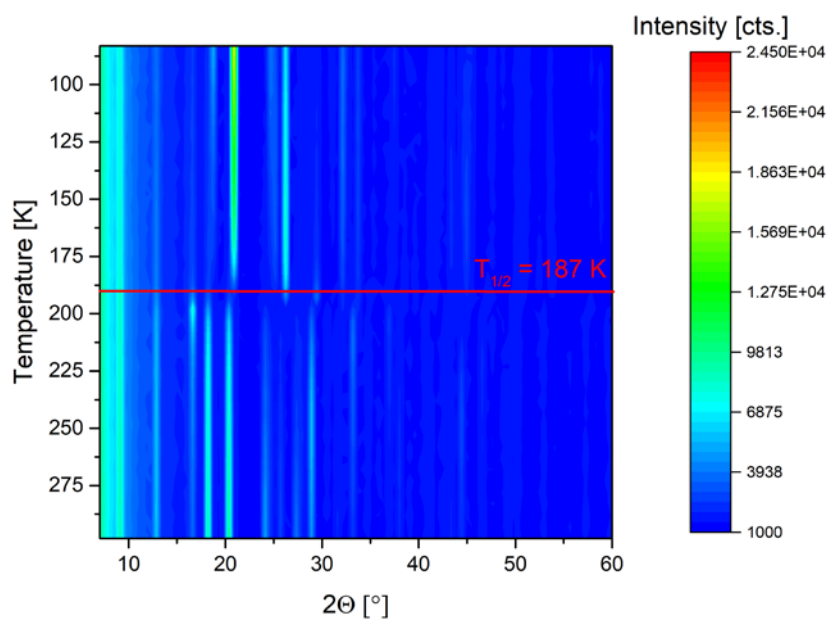


Fig. S19 Waterfall-plot of the temperature-dependent P-XRD data of **6**. The spin crossover associated volume work is observed at 187 K as shift of the peak positions. The inserted line is meant as a guide for the eye.

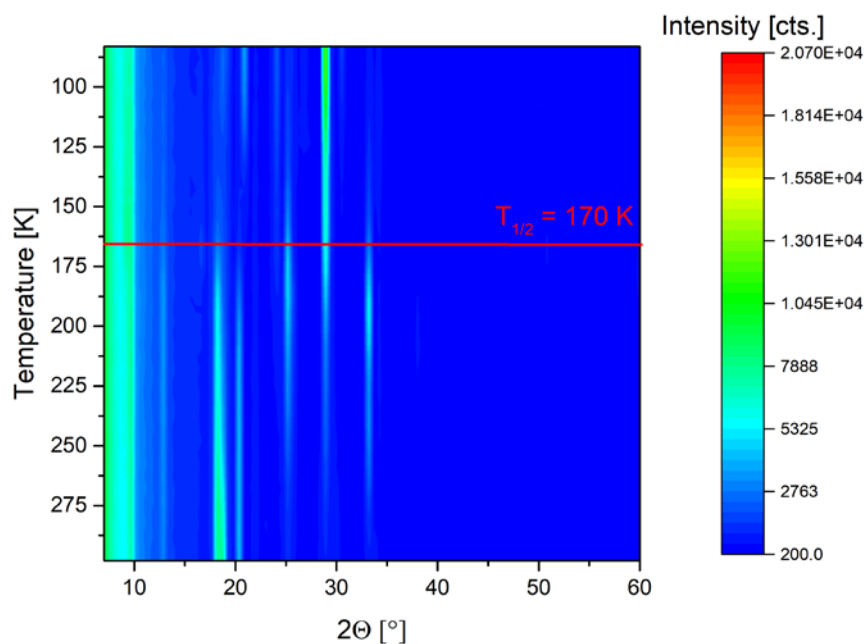


Fig. S20 Waterfall-plot of the temperature-dependent P-XRD data of **7**. The spin crossover associated volume work is observed at 170 K as shift of the peak positions. The inserted line is meant as a guide for the eye.

Computational details

The computational results presented were achieved using Gaussian 09 Rev.D01⁴ and visualized using GaussView 5.0.8.

The structures of the ligands were drawn using GaussView followed by a molecular mechanics structure optimization implemented in the software package.

For the complexes the molecular structures were imported from the single crystal X-ray data. One unit cell length of the iron(II) polymer chain was used as input molecule for the DFT calculations with a methyl tetrazole moiety as end group. High spin and low spin states were calculated applying the according spin multiplicity. The periodic boundary conditions implemented in Gaussian were not used due to repeated calculation failures and the impossibility to meet convergence criteria.

The calculations were run using density functional theory with the hybrid functional B3LYP⁵⁻⁷ for structure optimization to a ground state. Literature, dealing with DFT calculations of iron(II) spin crossover compounds, revealed that this functional is able to fit experimental data quite well.⁸⁻¹⁰ One possible adjustment to get better agreement to experimental data is the change of the exact exchange contribution from 20 % in B3LYP to 15 %, which is known as the B3LYP* functional.¹¹

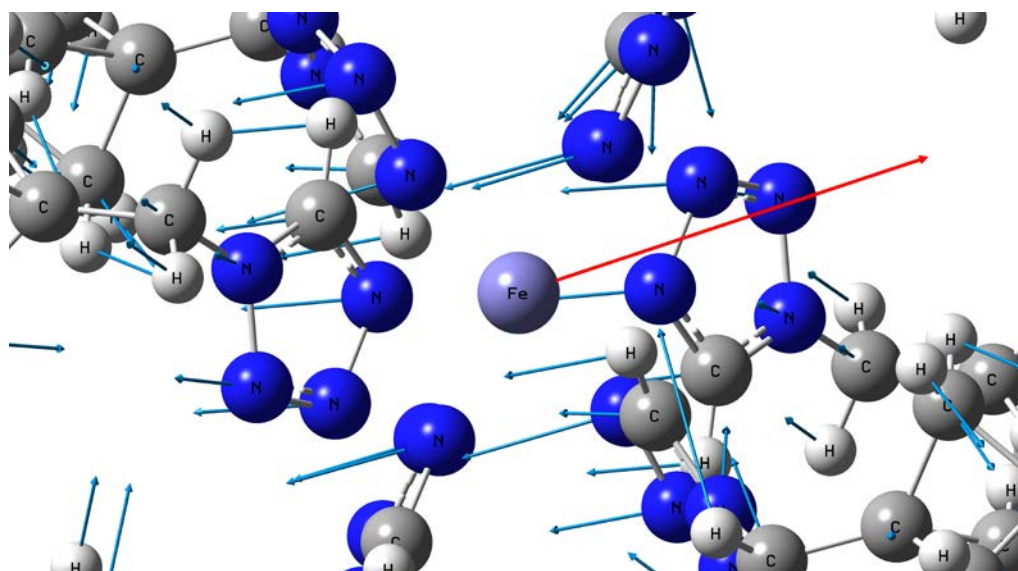
After an initial optimization towards a local minimum using the SDD basis set, the 6-311++g(d,p) valence triple zeta basis set¹² with polarization and diffuse functions on all atoms was used for refining the structure and calculation of vibrational modes to prove the local minimum.

Table S5 Comparison of experimental and theoretical bond-lengths

	Fe-Fe [Å]	Fe-N4 [Å]	N4-N3 [Å]	N3-N2 [Å]	N2-N1 [Å]	N4-C1 [Å]	C1-N1 [Å]	N1-C2 [Å]	C2-C3 [Å]	C3-C4 [Å]
5, HS	9.634	2.1864	1.3563	1.2909	1.3475	1.3128	1.3219	1.4684	1.5038	1.5459
5, LS	9.697	2.0207	1.3701	1.2831	1.3595	1.3230	1.3302	1.4665	1.5026	1.5494
6, HS	9.829	2.1788	1.3547	1.2840	1.3417	1.3204	1.3187	1.4678	1.4981	1.5436
6, LS	9.704	2.0255	1.3608	1.2897	1.3606	1.3191	1.3265	1.4561	1.5049	1.5494
Calc. HS	11.194	2.214	1.399	1.311	1.387	1.339	1.352	1.482	1.512	1.577
Calc. LS	10.780	2.010	1.400	1.310	1.384	1.341	1.351	1.483	1.512	1.577

Table S6 Comparison of experimental and theoretical bond-angles

	N4-Fe- N4[°]	N4-C1- N1 [°]	N1-C2- C3 [°]	C3-C4- C3 [°]
5, HS	92.16	108.67	109.67	73.95
5, LS	91.58	108.03	109.41	74.11
6, HS	91.59	108.50	110.19	73.86
6, LS	91.28	108.28	110.61	73.50
Calc. HS	89.8	108.3	115.4	74.1
Calc. LS	90.4	108.2	114.8	74.0

**Fig. S21** Characteristic LS-state iron motion in the N₆-octahedron at 252 cm⁻¹ (marked in red), overlapping with several vibrational modes of the propellane-spacer

References

1. A. F. Stepan, C. Subramanyam, I. V. Efremov, J. K. Dutra, T. J. O'Sullivan, K. J. DiRico, W. S. McDonald, A. Won, P. H. Dorff, C. E. Nolan, S. L. Becker, L. R. Pustilnik, D. R. Riddell, G. W. Kauffman, B. L. Kormos, L. Zhang, Y. Lu, S. H. Capetta, M. E. Green, K. Karki, E. Sibley, K. P. Atchison, A. J. Hallgren, C. E. Oborski, A. E. Robshaw, B. Sneed and C. J. O'Donnell, *J Med Chem*, 2012, **55**, 3414-3424.
2. W. L. F. Armarego, D. D. Perrin, Butterworth-Heinemann, Oxford, 1997.
3. I. Bruker Analytical X-ray Instruments, 2012.
4. M. J. Frisch, G. W. Trucks, H. B. Schlegel, G. E. Scuseria, M. A. Robb, J. R. Cheeseman, G. Scalmani, V. Barone, B. Mennucci, G. A. Petersson, H. Nakatsuji, M. Caricato, X. Li, H. P. Hratchian, A. F. Izmaylov, J. Bloino, G. Zheng, J. L. Sonnenberg, M. Hada, M. Ehara, K. Toyota, R. Fukuda, J. Hasegawa, M. Ishida, T. Nakajima, Y. Honda, O. Kitao, H. Nakai, T. Vreven, J. A. Montgomery Jr., J. E. Peralta, F. Ogliaro, M. J. Bearpark, J. Heyd, E. N. Brothers, K. N. Kudin, V. N. Staroverov, R. Kobayashi, J. Normand, K. Raghavachari, A. P. Rendell, J. C. Burant, S. S. Iyengar, J. Tomasi, M. Cossi, N. Rega, N. J. Millam, M. Klene, J. E. Knox, J. B. Cross, V. Bakken, C. Adamo, J. Jaramillo, R. Gomperts, R. E. Stratmann, O. Yazyev, A. J. Austin, R. Cammi, C. Pomelli, J. W. Ochterski, R. L. Martin, K. Morokuma, V. G. Zakrzewski, G. A. Voth, P. Salvador, J. J. Dannenberg, S. Dapprich, A. D. Daniels, Ö. Farkas, J. B. Foresman, J. V. Ortiz, J. Cioslowski and D. J. Fox, Gaussian, Inc.: Wallingford, CT, USA, 2009.
5. C. T. Lee, W. T. Yang and R. G. Parr, *Phys Rev B*, 1988, **37**, 785-789.
6. A. D. Becke, *J Chem Phys*, 1993, **98**, 5648-5652.
7. P. J. Stephens, F. J. Devlin, C. F. Chabalowski and M. J. Frisch, *J Phys Chem-Us*, 1994, **98**, 11623-11627.
8. M. Papai, G. Vanko, C. de Graaf and T. Rozgonyi, *J Chem Theory Comput*, 2013, **9**, 509-519.
9. J. Cirera and F. Paesani, *Inorg Chem*, 2012, **51**, 8194-8201.
10. A. Droghetti, D. Alfe and S. Sanvito, *J Chem Phys*, 2012, **137**.
11. M. Reiher, O. Salomon and B. A. Hess, *Theor Chem Acc*, 2001, **107**, 48-55.
12. Ditchfie.R, D. P. Miller and J. A. Pople, *J Chem Phys*, 1971, **54**, 4186-&.